# Highlights

**Constitutive equations for thermo-elasto-plastic metallic materials undergoing large temperature variations**

Charles Mareau

- A framework for the development of constitutive relations for metals is proposed
- The contributions of elasticity, plasticity and thermal expansions are included
- The temperature-dependence of thermomechanical properties is considered
- The proposed framework is well-suited for processes with large temperature variations

# Constitutive equations for thermo-elasto-plastic metallic materials undergoing large temperature variations

Charles Mareau

[a]*Arts et Metiers Institute of Technology, LAMPA, HESAM Université, 2, boulevard du Ronceray, Angers, 49035, , France*

**Abstract**

In the present work, a framework for the development of constitutive models for metallic materials in a thermomechanical context is proposed. Such a framework provides some guidelines to deal with processes involving large temperature variations, which is typical of manufacturing operations or severe service situations. The proposed framework relies on the additive decomposition of the logarithmic strain tensor to include the contributions of elasticity, plasticity and thermal expansion to deformation. Also, the classical internal variable concept is used to describe the history effects (e.g., hardening and recovery) associated with the development of plasticity. Particular attention is given to considering the impact of temperature on thermophysical properties. For the purpose of illustration, the proposed framework is used to build a constitutive model for polycrystalline copper. The resulting set of constitutive equations allows investigating the thermomechanical behavior of this specific material for some simple deformation histories. The corresponding results are finally used to evaluate the temperature-dependence of common thermophysical properties. The importance of the different heat sources that contribute to the heat diffusion equation is also discussed.

*Keywords:*
Thermomechanics, Constitutive model, Plasticity, Metals

## 1. Introduction

In many situations, the life of metallic products can be assimilated to a sequence of thermomechanical processes that affect both their shape and microstructure. Such a sequence includes manufacturing operations (e.g.,

forging, machining) as well as in-service loading events (e.g., fatigue, impact). As a result of thermomechanical couplings, some of these processes are difficult to apprehend in the sense that the motion and temperature histories are interdependent. While the impact of processing parameters can be evaluated with numerical or analytical simulation tools, reliable results require an accurate description of the constitutive behavior in a wide temperature range.

For metallic materials, the thermodynamics of irreversible processes with internal state variables (Valanis, 1971) provides a convenient framework for the development of constitutive models. Indeed, internal state variables, with the corresponding evolution equations, allow constructing a large variety of constitutive models that consider history effects (Maugin and Muschik, 1994). In contrast with formulations relying on history functionals, internal variable-based constitutive models can easily be enriched to include additional effects resulting from different physical phenomena affecting the behavior of materials (Papenfuß, 2020). Such a framework has notably been used to construct an important number of thermo-elasto-plastic constitutive models in the context of either infinitesimal (Houlsby and Puzrin, 2000; Benallal and Bigoni, 2004; Egner and Egner, 2014) or finite (Simo and Miehe, 1992; Xiao *et al.*, 2007; Mareau, 2020) strains. Since the aforementioned models are compatible with the fundamental laws of thermodynamics, they allow (i) computing the different heat sources that control the temperature evolution and (ii) considering the impact of temperature on the thermomechanical behavior. However, such constitutive models often ignore the temperature-dependence of thermophysical properties such as the specific heat capacity or the thermal expansion tensor. As a consequence, these constitutive models are limited to quasi-isothermal processes, i.e., with small temperature variations. However, many practical applications of metallic materials involve important temperature variations. For instance, as a result of heat dissipation caused by plasticity and friction, the temperature in the cutting zone during machining operations can increase from room temperature to a few hundreds of degrees (Shaw, 2005; Harzallah *et al.*, 2018). Also, the heat treatment of metallic materials often involve significant temperature variations, hence important changes of thermophysical properties (Zeng *et al.*, 2021).

In the present manuscript, a general framework that allows describing the thermo-elasto-plastic behavior of metallic materials under arbitrary temperature variations is proposed. The additive decomposition of the logarithmic

strain tensor[1] (Hencky, 1928) into elastic, thermal and plastic contributions is first briefly presented. The general form of constitutive equations, which relies on the internal variable concept to consider the history effects (e.g., hardening, recovery) that affect the development of plasticity, is then detailed. Particular attention is given to considering the impact of temperature on thermophysical properties. Specifically, some strategies that comply with the restrictions from the third law of thermodynamics are presented to include the temperature-dependence of common thermophysical properties. For the purpose of illustration, the proposed framework is finally used to build a set of constitutive relations for polycrystalline copper.

## 2. Constitutive equations

### *2.1. Decomposition of the logarithmic strain tensor*

The present work aims at presenting a general strategy to develop constitutive equations for thermo-elasto-plastic metallic solids. For this purpose, a material point with initial position $\boldsymbol{X}$ is considered. For such a material point, the position $\boldsymbol{x}$ and temperature $T$ at time $t$ are obtained from the functions $\boldsymbol{\xi}$ and $\theta$ that define the motion and temperature histories with:

$$\boldsymbol{x} = \boldsymbol{\xi}[\boldsymbol{X}, t] \text{ and } T = \theta[\boldsymbol{X}, t] \tag{1}$$

For any regular material point, the deformation gradient tensor $\boldsymbol{F}$ is given by:

$$\boldsymbol{F} = \boldsymbol{\xi} \otimes \boldsymbol{\nabla}_0 \tag{2}$$

$$= \boldsymbol{R} \cdot \boldsymbol{U} \tag{3}$$

where $\boldsymbol{R}$ and $\boldsymbol{U}$ are respectively the rotation tensor and right stretch tensor obtained from the polar decomposition of the deformation gradient tensor. Also, $\boldsymbol{\nabla}_0$ is the differential operator indicating differentiation with respect to the initial position $\boldsymbol{X}$. For the construction of constitutive relations, the logarithmic strain tensor $\boldsymbol{E}$ is used as a strain measure. The logarithmic strain tensor is obtained from the right stretch tensor $\boldsymbol{U}$ according to:

$$\boldsymbol{E} = \ln[\boldsymbol{U}] \tag{4}$$

[1]The logarithmic strain tensor is also known as the Hencky or true strain tensor.

The logarithmic strain tensor can be additively decomposed to include the contributions of the different deformation mechanisms. Such a decomposition is adopted in different implementations of elastic-plastic constitutive models in the context of finite strains, e.g., (Papadopoulos and Lu, 2001; Miehe *et al.*, 2002; Sansour and Wagner, 2001). As discussed by Miehe *et al.* (2002), the additive decomposition of the logarithmic strain tensor provides numerical results that are close to those obtained with the reference framework of multiplicative plasticity. For thermo-elasto-plastic solids, the strain tensor includes elastic (subscript $e$), thermal (subscript $th$) and plastic (subscript $p$) contributions:

$$\boldsymbol{E} = \boldsymbol{E}_e + \boldsymbol{E}_{th} + \boldsymbol{E}_p \tag{5}$$

The thermal contribution, which solely depends on the temperature, is obtained from the stress-free thermal expansion tensor $\bar{\boldsymbol{\alpha}}$ with:

$$\boldsymbol{E}_{th} = \int_{T_0}^{T} \bar{\boldsymbol{\alpha}}[T'] \; dT' \tag{6}$$

where $T_0$ is a reference temperature for which the thermal strain tensor vanishes.

*2.2. Logarithmic stress tensor*

During a deformation process, the specific power developed by internal forces $p$ is obtained from:

$$p = \frac{1}{\varrho_0} \boldsymbol{P} : \dot{\boldsymbol{F}} \tag{7}$$

where $\varrho_0$ is the mass density in the initial configuration and $\boldsymbol{P}$ is the first Piola-Kirchoff stress tensor.

For the construction of constitutive relations, it is preferable to work with the stress tensor $\boldsymbol{\Sigma}$, which is the power-conjugate to the logarithmic strain rate tensor in the sense that:

$$p = \frac{1}{\varrho_0} \boldsymbol{\Sigma} : \dot{\boldsymbol{E}} \tag{8}$$

Adopting the terminology of Caminero *et al.* (2011), the tensor $\boldsymbol{\Sigma}$ is referred to as the logarithmic stress tensor in the following. Also, since the above relations should be equivalent, the first Piola-Kirchoff and logarithmic stress tensors are related to each other according to:

$$\boldsymbol{P} = \boldsymbol{R} \cdot (\boldsymbol{\Sigma} : \mathbb{M}) \tag{9}$$

| Primal state variable | Dual state variable |
|---|---|
| $\boldsymbol{E}$ | $\boldsymbol{\Sigma}$ |
| $T$ | $-s$ |
| $\boldsymbol{E}_p$ | $-\boldsymbol{\Sigma}$ |
| $\boldsymbol{A}$ | $\boldsymbol{\chi}$ |
| $Z$ | $R$ |

Table 1: List of primal and dual state variables.

where the fourth-rank tensor $\mathbb{M}$ is obtained from:

$$\mathbb{M} = \frac{\partial \boldsymbol{E}}{\partial \boldsymbol{U}} \tag{10}$$

*2.3. State equations*

At a given time $t$, the state of the material point is uniquely defined from a set of state variables that are listed in Table 1 with their corresponding dual variables. The external state variables are the total strain tensor $\boldsymbol{E}$ and the absolute temperature $T$. For the description of the deformation behavior, some additional internal state variables are introduced. First, the plastic strain tensor $\boldsymbol{E}_p$, which depends on the thermomechanical history, is treated as a tensorial internal variable. Also, to consider hardening, a scalar and a tensorial hardening variable, denoted by $Z$ and $\boldsymbol{A}$, are introduced[2]. While the former allows incorporating the contribution of isotropic hardening, the latter allows describing the effects of kinematic hardening.

Using the above set of state variables, the specific free energy $f$ is decomposed into three contributions:

$$f = f_e + f_{th} + f_h \tag{11}$$

The elastic contribution $f_e$ is obtained from:

$$f_e = \frac{1}{2\varrho_0} \boldsymbol{E}_e : \mathbb{C} : \boldsymbol{E}_e \tag{12}$$

[2]Though this option is not explored here for simplicity, the present framework can easily be extended to consider multiple (isotropic or kinematic) hardening variables.

where $\mathbb{C}$ is the temperature-dependent stiffness tensor. The thermal contribution to free energy $f_{th}$ solely depends on temperature :

$$f_{th} = -\int_{T_0}^{T} \left( \int_{T_0}^{T'} \frac{\bar{c}_p}{T''} dT'' \right) dT' - s_0 \left( T - T_0 \right) + f_0 \tag{13}$$

In the above equation, $f_0$ and $s_0$ are the specific free energy and entropy at the reference temperature in the absence of elastic strain and hardening. Also, as discussed hereafter, $\bar{c}_p$ is the specific heat capacity at constant stress that would be obtained in the absence of applied stress and hardening. Finally, the contribution of hardening to free energy $f_h$ includes the separate effects of isotropic hardening and kinematic hardening:

$$f_h = \frac{1}{2\varrho_0} H Z^2 + \frac{1}{2\varrho_0} \boldsymbol{A} : \mathbb{K} : \boldsymbol{A} \tag{14}$$

where $\mathbb{K}$ is the temperature-dependent kinematic hardening moduli tensor and $H$ is the temperature-dependent isotropic hardening modulus.

In the absence of viscous contribution, the logarithmic stress tensor $\boldsymbol{\Sigma}$ is given by:

$$\boldsymbol{\Sigma} = \varrho_0 \frac{\partial f}{\partial \boldsymbol{E}} = -\varrho_0 \frac{\partial f}{\partial \boldsymbol{E}_p} \tag{15}$$

$$= \mathbb{C} : \boldsymbol{E}_e \tag{16}$$

To incorporate the effect of kinematic hardening, it is convenient to introduce the backstress tensor $\boldsymbol{\chi}$, which is the conjugate variable of the kinematic hardening variable $\boldsymbol{A}$. The corresponding state equation is:

$$\boldsymbol{\chi} = \varrho_0 \frac{\partial f}{\partial \boldsymbol{A}} \tag{17}$$

$$= \mathbb{K} : \boldsymbol{A} \tag{18}$$

The differentiation of Equation (14) with respect to the isotropic hardening variable provides the state equation for the yield stress increase $R$:

$$R = \varrho_0 \frac{\partial f}{\partial Z} \tag{19}$$

$$= HZ \tag{20}$$

The specific entropy $s$ is obtained from the specific free energy $f$ with:

$$s = -\frac{\partial f}{\partial T} \tag{21}$$

$$\begin{aligned} &= \int_{T_0}^{T} \frac{\bar{c}_p}{T'} dT' + \frac{1}{\varrho_0} \boldsymbol{E}_e : \mathbb{C} : \bar{\boldsymbol{\alpha}} - \frac{1}{2\varrho_0} \boldsymbol{E}_e : \frac{\partial \mathbb{C}}{\partial T} : \boldsymbol{E}_e \\ &- \frac{1}{2\varrho_0} \frac{\partial H}{\partial T} Z^2 - \frac{1}{2\varrho_0} \boldsymbol{A} : \frac{\partial \mathbb{K}}{\partial T} : \boldsymbol{A} + s_0 \end{aligned} \tag{22}$$

To comply with the third law of thermodynamics, the following temperature-dependent quantities should vanish at absolute zero:

$$\bar{c}_p[0] = 0,\ \bar{\boldsymbol{\alpha}}[0] = \boldsymbol{0},\ \left.\frac{\partial \mathbb{C}}{\partial T}\right|_0 = \mathbb{O},\ \left.\frac{\partial \mathbb{K}}{\partial T}\right|_0 = \mathbb{O},\ \left.\frac{\partial H}{\partial T}\right|_0 = 0 \tag{23}$$

The specific internal energy $e$, which, upon integration, allows evaluating the total internal energy of the system of interest, is obtained from the different state variables with:

$$e = f + sT \tag{24}$$

$$\begin{aligned} &= \frac{1}{\varrho_0} \boldsymbol{E}_e : \mathbb{C} : \bar{\boldsymbol{\alpha}} T + \frac{1}{2\varrho_0} \boldsymbol{E}_e : \left( \mathbb{C} - \frac{\partial \mathbb{C}}{\partial T} T \right) : \boldsymbol{E}_e \\ &+ \frac{1}{2\varrho_0} \left( H - \frac{\partial H}{\partial T} T \right) Z^2 + \frac{1}{2\varrho_0} \boldsymbol{A} : \left( \mathbb{K} - \frac{\partial \mathbb{K}}{\partial T} T \right) : \boldsymbol{A} \\ &+ \int_{T_0}^{T} \bar{c}_p \, dT' + e_0 \end{aligned} \tag{25}$$

where $e_0 = f_0 + s_0 T_0$ is the specific internal energy at the reference temperature in the absence of elastic strain and hardening.

*2.4. Thermal expansion tensor and specific heat capacity*

According to Equation (16), the total logarithmic strain tensor $\boldsymbol{E}$ can be expressed as a function of the logarithmic stress tensor $\boldsymbol{\Sigma}$ with:

$$\boldsymbol{E} = \mathbb{S} : \boldsymbol{\Sigma} + \boldsymbol{E}_{th} + \boldsymbol{E}_p \tag{26}$$

where $\mathbb{S} = \mathbb{C}^{-1}$ is the temperature-dependent elastic compliance tensor. The thermal expansion tensor $\boldsymbol{\alpha}$ is obtained by differentiating the total strain

tensor with respect to temperature for a fixed stress state and a fixed internal state, which leads to[3]:

$$\boldsymbol{\alpha} = \left.\frac{\partial \boldsymbol{E}}{\partial T}\right|_{\boldsymbol{\Sigma},\text{int}} \tag{27}$$

$$= \frac{\partial \mathbb{S}}{\partial T} : \boldsymbol{\Sigma} + \bar{\boldsymbol{\alpha}} \tag{28}$$

$$= -\mathbb{S} : \frac{\partial \mathbb{C}}{\partial T} : \boldsymbol{E}_e + \bar{\boldsymbol{\alpha}} \tag{29}$$

The above equation indicates that the current thermal expansion tensor $\boldsymbol{\alpha}$ is equal to the stress-free thermal expansion tensor $\bar{\boldsymbol{\alpha}}$ in the absence of applied stress or when stiffness properties do not depend on temperature.

For a fixed internal state and a constant strain state, the differentiation of the specific entropy with respect to temperature leads to the expression of the specific heat capacity at constant strain $c_v$ with:

$$c_v = T \left.\frac{\partial s}{\partial T}\right|_{\boldsymbol{E},\text{int}} \tag{30}$$

$$\begin{aligned} &= \bar{c}_v + \frac{2}{\varrho_0}\boldsymbol{E}_e : \frac{\partial \mathbb{C}}{\partial T} : \bar{\boldsymbol{\alpha}} T + \frac{1}{\varrho_0}\boldsymbol{E}_e : \mathbb{C} : \frac{\partial \bar{\boldsymbol{\alpha}}}{\partial T} T \\ &- \frac{1}{2\varrho_0}\boldsymbol{E}_e : \frac{\partial^2 \mathbb{C}}{\partial T^2} : \boldsymbol{E}_e T - \frac{1}{2\varrho_0}\frac{\partial^2 H}{\partial T^2} Z^2 T \\ &- \frac{1}{2\varrho_0}\boldsymbol{A} : \frac{\partial^2 \mathbb{K}}{\partial T^2} : \boldsymbol{A} T \end{aligned} \tag{31}$$

where $\bar{c}_v = \bar{c}_p - \bar{\boldsymbol{\alpha}} : \mathbb{C} : \bar{\boldsymbol{\alpha}} T/\varrho_0$ is the specific heat capacity at constant strain that would be obtained in the absence of applied stress (i.e., $\boldsymbol{E}_e = \boldsymbol{0}$) and without any contribution from hardening (i.e., $\boldsymbol{A} = \boldsymbol{0}$ and $Z = 0$).

From an experimental point of view, common thermoanalytical techniques, such as differential scanning calorimetry, provide the specific heat capacity at constant stress rather than constant strain. The specific heat

[3]The subscript "int" is used to emphasize that the differentiation is carried out at a constant internal state, i.e., for a fixed plastic strain tensor and fixed kinematic and isotropic hardening variables.

capacity at constant stress $c_p$ is given by:

$$c_p = T\frac{\partial s}{\partial T}\bigg|_{\boldsymbol{\Sigma},\text{int}} \tag{32}$$

$$= c_v + \frac{1}{\varrho_0}\boldsymbol{\alpha} : \mathbb{C} : \boldsymbol{\alpha} T \tag{33}$$

$$\begin{aligned} &= \bar{c}_p - \frac{1}{\varrho_0}\boldsymbol{E}_e : \frac{\partial \mathbb{C}}{\partial T} : \boldsymbol{\alpha} T + \frac{1}{\varrho_0}\boldsymbol{E}_e : \mathbb{C} : \frac{\partial \boldsymbol{\alpha}}{\partial T} T \\ &+ \frac{1}{2\varrho_0}\boldsymbol{E}_e : \frac{\partial^2 \mathbb{C}}{\partial T^2} : \boldsymbol{E}_e T - \frac{1}{\varrho_0}\boldsymbol{E}_e : \frac{\partial \mathbb{C}}{\partial T} : \mathbb{S} : \frac{\partial \mathbb{C}}{\partial T} : \boldsymbol{E}_e T \\ &- \frac{1}{2\varrho_0}\frac{\partial^2 H}{\partial T^2} Z^2 T - \frac{1}{2\varrho_0}\boldsymbol{A} : \frac{\partial^2 \mathbb{K}}{\partial T^2} : \boldsymbol{A} T \end{aligned} \tag{34}$$

According to the above equation, the reference specific heat capacity at constant stress $\bar{c}_p$ can be determined from thermoanalytical experiments conducted in the absence of applied stress and hardening.

*2.5. Evolution equations*

*2.5.1. Dissipation source*

According to classical thermodynamics, the specific dissipation source $d$ is given by:

$$d = \frac{1}{\varrho_0}\boldsymbol{\Sigma} : \dot{\boldsymbol{E}} - \dot{a} - s\dot{T} - \frac{1}{\varrho_0}\boldsymbol{Q} \cdot \frac{\boldsymbol{\nabla}_0 T}{T} \tag{35}$$

where $\boldsymbol{Q}$ is the heat flux vector in the reference configuration. Using the state equations (16), (18), (20) and (22), the specific dissipation source is conveniently written under the following form:

$$d = \frac{1}{\varrho_0}\boldsymbol{\Sigma} : \dot{\boldsymbol{E}}_p - \frac{1}{\varrho_0} R\dot{Z} - \frac{1}{\varrho_0}\boldsymbol{\chi} : \dot{\boldsymbol{A}} - \frac{1}{\varrho_0}\boldsymbol{Q} \cdot \frac{\boldsymbol{\nabla}_0 T}{T} \tag{36}$$

The specific dissipation source can be separated into two contributions such that:

$$d = d_{in} + d_{th} \tag{37}$$

with:

$$d_{in} = \frac{1}{\varrho_0}\boldsymbol{\Sigma} : \dot{\boldsymbol{E}}_p - \frac{1}{\varrho_0} R\dot{Z} - \frac{1}{\varrho_0}\boldsymbol{\chi} : \dot{\boldsymbol{A}} \tag{38}$$

$$d_{th} = -\frac{1}{\varrho_0}\boldsymbol{Q} \cdot \frac{\boldsymbol{\nabla}_0 T}{T} \tag{39}$$

As indicated by the above equations, the thermal dissipation source $d_{th}$ includes the contribution of heat conduction while the intrinsic dissipation source $d_{in}$ is the result of the microstructural changes associated with plasticity and hardening.

To comply with the restrictions of the second law of thermodynamics, it is common to require both the thermal and intrinsic dissipation sources to be non-negative (Nguyen, 2000):

$$d_{th} \geq 0 \text{ and } d_{in} \geq 0 \tag{40}$$

A locally reversible process corresponds to the specific case where the thermal and intrinsic dissipation sources both vanish.

The Taylor-Quinney coefficient (Taylor, 1934) is commonly used as a measure of the efficiency of the dissipation of mechanical power into heat. Following the terminology of Rittel *et al.* (2017), the differential Taylor-Quinney coefficient $\beta$ is defined as the ratio between the intrinsic dissipation source and the specific plastic work rate:

$$\beta = \varrho_0 \frac{d_{in}}{\boldsymbol{\Sigma} : \dot{\boldsymbol{E}}_p} \tag{41}$$

$$= \frac{\boldsymbol{\Sigma} : \dot{\boldsymbol{E}}_p - R\dot{Z} - \boldsymbol{\chi} : \dot{\boldsymbol{A}}}{\boldsymbol{\Sigma} : \dot{\boldsymbol{E}}_p} \tag{42}$$

The above equation indicates that in the absence of hardening, the plastic work rate is entirely dissipated into heat, in which case the Taylor-Quinney coefficient $\beta$ takes a unit value. Depending on the evolution of a material point, the hardening contribution to the intrinsic dissipation source may participate in energy storage or energy dissipation. The former case typically corresponds to the situation where internal energy increases because crystallographic defects are created. The latter case is encountered when static or dynamic recovery phenomena contribute to the release of internal energy.

*2.5.2. Evolution equations*

The expression of the specific dissipation source (36) indicates that the constitutive model must include some evolution equations for the plastic strain rate tensor, the kinematic variable rate, the isotropic variable rate and the heat flux density vector. Such evolution equations should comply with the second law of thermodynamics, i.e., the thermal and intrinsic dissipation sources must be non-negative.

For most metallic alloys, the heat flux vector is commonly obtained from the Fourier's law of heat conduction:

$$\boldsymbol{Q} = -\boldsymbol{\kappa} \cdot \boldsymbol{\nabla}_0 T \tag{43}$$

where $\boldsymbol{\kappa}$ is the temperature-dependent heat conductivity tensor. Since heat conduction is impacted by the concentration of defects (e.g., Wasserbäh (1978)), one may assume that the heat conductivity tensor also depends on the isotropic hardening variable. Also, for the thermal contribution to the dissipation source to be non-negative, the heat conductivity tensor should be positive semi-definite.

To determine whether the conditions for plastic flow are met or not, it is convenient to introduce a first order homogeneous function $\sigma$ that returns an equivalent stress $\Sigma_{eq}$ from the effective stress tensor, i.e., $\boldsymbol{\Sigma} - \boldsymbol{\chi}$, with:

$$\Sigma_{eq} = \sigma \left[ \boldsymbol{\Sigma} - \boldsymbol{\chi} \right] \tag{44}$$

To construct the evolution equation for the plastic strain rate tensor, most plasticity theories use the following decomposition:

$$\dot{\boldsymbol{E}}_p = \dot{P} \boldsymbol{N} \tag{45}$$

where $\dot{P}$ is the plastic multiplier, which measures the intensity of plastic flow, and $\boldsymbol{N}$ is the plastic flow direction. When the normality rule is adopted, the plastic flow direction is given by:

$$\boldsymbol{N} = \frac{\partial \Sigma_{eq}}{\partial \boldsymbol{\Sigma}} \tag{46}$$

The evolution of the isotropic hardening variable is controlled by two contributions denoted by $\dot{Z}_p$ and $\dot{Z}_r$. The contribution $\dot{Z}_p$ includes the effects of strain hardening and dynamic recovery while the contribution $\dot{Z}_r$ incorporates the effect of static recovery. The evolution equation for the isotropic variable thus takes the following form:

$$\dot{Z} = \dot{Z}_p + \dot{Z}_r \tag{47}$$

with:

$$\dot{Z}_p = F_p[\boldsymbol{E}, \boldsymbol{E}_p, \boldsymbol{A}, Z, T] \dot{P} \tag{48}$$

$$\dot{Z}_r = F_r[\boldsymbol{E}, \boldsymbol{E}_p, \boldsymbol{A}, Z, T] \tag{49}$$

While the contribution of strain hardening and dynamic recovery necessarily vanishes when the conditions for plastic flow are not met, that of static recovery may exist in the absence of plastic flow.

The evolution equation for the kinematic hardening variable displays a form similar to that of the isotropic hardening variable. Specifically, the evolution of the kinematic hardening variable depends on a plastic term $\dot{\boldsymbol{A}}_p$ and a static recovery term $\dot{\boldsymbol{A}}_r$, whose effect is expected to be significant at high temperature:

$$\dot{\boldsymbol{A}} = \dot{\boldsymbol{A}}_p + \dot{\boldsymbol{A}}_r \tag{50}$$

with:

$$\dot{\boldsymbol{A}}_p = \boldsymbol{G}_p[\boldsymbol{E}, \boldsymbol{E}_p, \boldsymbol{A}, Z, T]\dot{P} \tag{51}$$

$$\dot{\boldsymbol{A}}_r = \boldsymbol{G}_r[\boldsymbol{E}, \boldsymbol{E}_p, \boldsymbol{A}, Z, T] \tag{52}$$

As for the evolution equation for the isotropic hardening variable, the plastic contribution vanishes when the conditions for plastic flow are not met.

*2.6. Heat diffusion equation*

For each material point, the temperature evolution is obtained from the heat diffusion equation whose derivation for the specific case of thermo-elasto-plastic solids is detailed hereafter.

According to the first law of thermodynamics, the evolution of the specific internal energy $e$ is given by:

$$\dot{e} = \frac{1}{\varrho_0}\boldsymbol{\Sigma} : \dot{\boldsymbol{E}} - \frac{1}{\varrho_0}\boldsymbol{\nabla}_0 \cdot \boldsymbol{Q} + r \tag{53}$$

Also, from the relation between the specific internal energy, the specific free energy, the specific entropy and the absolute temperature, one obtains:

$$\dot{e} = \dot{a} + T\dot{s} + s\dot{T} \tag{54}$$

Combining the above equations and using the expression of the specific intrinsic dissipation source leads to:

$$T\dot{s} = \frac{1}{\varrho_0}\boldsymbol{\Sigma} : \dot{\boldsymbol{E}} - \frac{1}{\varrho_0}\boldsymbol{\nabla}_0 \cdot \boldsymbol{Q} + r - \dot{a} - s\dot{T} \tag{55}$$

$$= d_{in} - \frac{1}{\varrho_0}\boldsymbol{\nabla}_0 \cdot \boldsymbol{Q} + r \tag{56}$$

The evolution of the specific entropy is given by:

$$\dot{s} = \frac{\partial s}{\partial T}\dot{T} + \frac{\partial s}{\partial \boldsymbol{E}} : \dot{\boldsymbol{E}} + \frac{\partial s}{\partial \boldsymbol{E}_p} : \dot{\boldsymbol{E}}_p + \frac{\partial s}{\partial \boldsymbol{A}} : \dot{\boldsymbol{A}} + \frac{\partial s}{\partial Z}\dot{Z} \tag{57}$$

$$= \frac{\partial s}{\partial T}\dot{T} + \frac{\partial s}{\partial \boldsymbol{E}_e} : \left(\dot{\boldsymbol{E}} - \dot{\boldsymbol{E}}_p\right) + \frac{\partial s}{\partial \boldsymbol{A}} : \dot{\boldsymbol{A}} + \frac{\partial s}{\partial Z}\dot{Z} \tag{58}$$

$$= \frac{1}{T}\left(c_v\dot{T} - \varphi_\theta - \varphi_{ic}\right) \tag{59}$$

In the above equation, $\varphi_\theta$ is the specific thermoelastic heat source:

$$\varphi_\theta = -T\frac{\partial s}{\partial \boldsymbol{E}_e} : \left(\dot{\boldsymbol{E}} - \dot{\boldsymbol{E}}_p\right) \tag{60}$$

$$= -\frac{1}{\varrho_0}T\boldsymbol{\alpha} : \left(\dot{\boldsymbol{\Sigma}} + \mathbb{C} : \boldsymbol{\alpha}\dot{T}\right) \tag{61}$$

Also, $\varphi_{ic}$ is the internal coupling source that results from the dependence of the internal state on the absolute temperature. In the present context, the internal state is represented by the isotropic and kinematic hardening variables. The resulting expression of the internal coupling source is:

$$\varphi_{ic} = -T\frac{\partial s}{\partial \boldsymbol{A}} : \dot{\boldsymbol{A}} - T\frac{\partial s}{\partial Z}\dot{Z} \tag{62}$$

$$= \frac{1}{\varrho_0}T\frac{\partial \boldsymbol{\chi}}{\partial T} : \dot{\boldsymbol{A}} + \frac{1}{\varrho_0}T\frac{\partial R}{\partial T}\dot{Z} \tag{63}$$

With the above definitions of the different heat sources, the heat diffusion equation is conveniently written as:

$$c_v\dot{T} = d_{in} + \varphi_\theta + \varphi_{ic} - \frac{1}{\varrho_0}\boldsymbol{\nabla}_0 \cdot \boldsymbol{Q} + r \tag{64}$$

The above equation indicates that the temperature evolution of a material point is controlled by heat transfer ($-\boldsymbol{\nabla}_0 \cdot \boldsymbol{Q}/\varrho_0 + r$), heat dissipation caused by irreversible microstructural changes ($d_{in}$) and heat sources due to the impact of temperature on the stress state ($\varphi_\theta$) and hardening ($\varphi_{ic}$).

*2.7. Temperature dependence of thermomechanical properties*

For most metallic materials, physical properties such as the specific heat capacity or the thermal conductivity vary significantly with temperature. As

a result, for applications with important temperature variations, the temperature dependence of these properties must be considered to accurately describe the thermomechanical behavior of metallic materials. Different strategies to describe the impact of temperature on thermomechanical properties are proposed in this section.

*2.7.1. Specific heat capacity*

For most metallic materials, the impact of temperature on the specific heat capacity at zero stress is correctly described with a function that includes two contributions:

$$\bar{c}_p = C_\infty \left(\frac{T}{T_d}\right)^3 \int_0^{T_d/T} \frac{x^4 \exp x}{(\exp x - 1)^2} dx + \sum_{i=1}^{n_c} C_i T^i \tag{65}$$

The temperature-dependent phonon contribution to the specific heat is described according to the Debye model (Debye, 1912). It involves two material parameters: the Debye temperature $T_d$ and the asymptotic specific heat capacity $C_\infty$[4]. The polynomial function of order $n_c$ includes the contribution of free electrons as well as the deviations from the Debye model. For such a polynomial function, the coefficient of the term of order $i$ is denoted by $C_i$. Also, to comply with the third law of thermodynamics, the polynomial function must be zero at origin, i.e., it should not include a zeroth order term.

The experimental values of the specific heat capacity at constant stress are compared with those obtained from Equation (65) for different metallic materials in Figure 1. The fitting function provides a reasonable description of experimental data for most materials in both low and high temperature regimes. A notable exception is the Ti6Al4V alloy for which, as a result of the $\alpha \rightarrow \beta$ phase transition, significant discrepancies are observed around the $\beta$ transus temperature. This specific example highlights the need to incorporate additional contributions in Equation (65) when solid state phase transitions exist.

*2.7.2. Thermal expansion coefficient*

As discussed by Tang *et al.* (2021), there is a strong connection between the heat capacity at constant stress and the thermal expansion coefficient for

[4]According to the Debye model, the asymptotic specific heat capacity is given by $C_\infty = 3R/M$ where $R$ is the molar gas constant and $M$ is the molar mass.

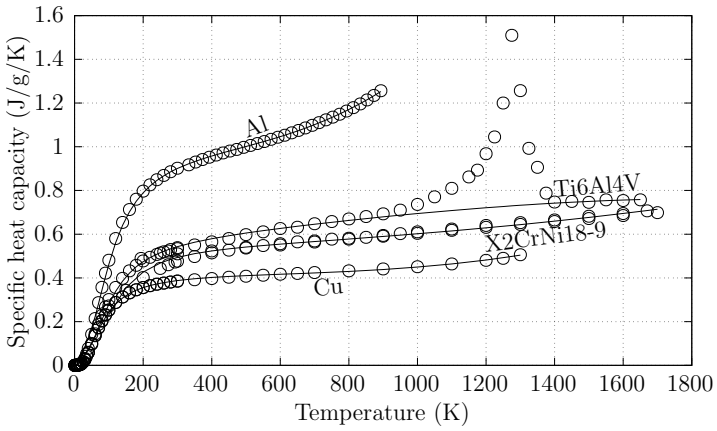


Figure 1: Temperature dependence of the specific heat capacity of several metallic materials. Dots correspond to the experimental data taken from (Miločević and Aleksić, 2012; Ziegler *et al.*, 1963; Kim, 1975; Touloukian and Ho, 1977; White and Collocott, 1984; Brooks and Bingham, 1968). Numerical data obtained from Equation (65) is represented with solid lines.

many solid materials, including pure metals. As a consequence, the thermal expansion coefficient of most metallic materials is well depicted by a relation similar to that used for the specific heat capacity:

$$\bar{\alpha} = A_\infty \left(\frac{T}{T_d}\right)^3 \int_0^{T_d/T} \frac{x^4 \exp x}{(\exp x - 1)^2} dx + \sum_{i=1}^{n_\alpha} A_i T^i \tag{66}$$

In the above equation, $A_\infty$ is asymptotic value of the thermal expansion coefficient while the $A_i$ coefficient controls the effect of the $i$th order term of the polynomial contribution.

For the purpose of illustration, the thermal expansion coefficients of different metallic materials are plotted as a function of temperature in Figure 2. The values obtained from Equation (66) are also provided. According to the results, the impact of temperature on the thermal expansion coefficient is correctly depicted with Equation (66). Specifically, the thermal thermal expansion approaches a zero value when the absolute temperature tends toward absolute zero, which is in agreement with the third law of thermodynamics. Also, it is worth mentioning that, as for the specific heat capacity, additional contributions to the thermal expansion coefficient should be included to reproduce the effect of phase transitions. As illustrated by the work of (Zhang

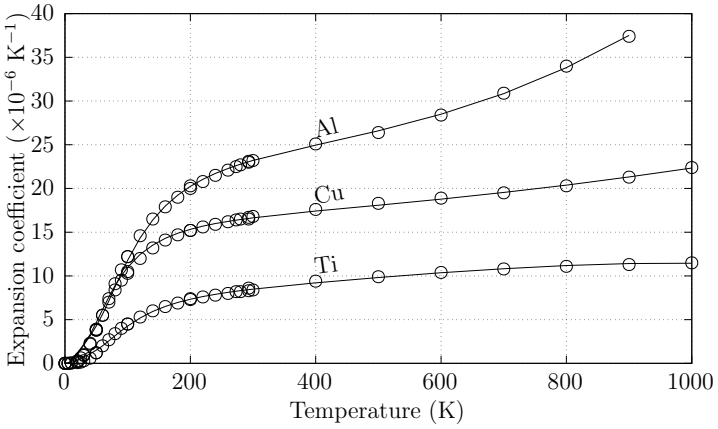


Figure 2: Temperature dependence of the linear thermal expansion coefficient of several metallic materials. Dots correspond to the experimental data taken from (Johnson, 1960; Touloukian *et al.*, 1975). Numerical data obtained from Equation (66) is represented with solid lines.

and Baxevanis, 2022), this effect is particularly visible in shape memory alloys.

*2.7.3. Thermal conductivity*

For pure metals, the impact of temperature on heat conductivity is usually well described by the following equation, which is a modified version of the model proposed by Cezairliyan and Touloukian (1965):

$$\kappa = \left( \frac{1}{\kappa_p} + \frac{1}{\kappa_d} + K_7 \frac{1}{\kappa_d + \kappa_p} \right)^{-1} \tag{67}$$

where the contribution $\kappa_d$ (respectively $\kappa_p$) accounts for the effect of electron-defect (respectively electron-phonon) interactions. These temperature-dependent contributions are described according to:

$$\kappa_d = \frac{T}{K_0} \tag{68}$$

$$\kappa_p = \frac{1 + K_1 K_3 T^{K_2+K_4} \exp\left[-(K_5/T)^{K_6}\right]}{K_1 T^{K_2}} \tag{69}$$

In the above equations, the $K_i$ coefficients (with $i = 0$ to 7) are material parameters.

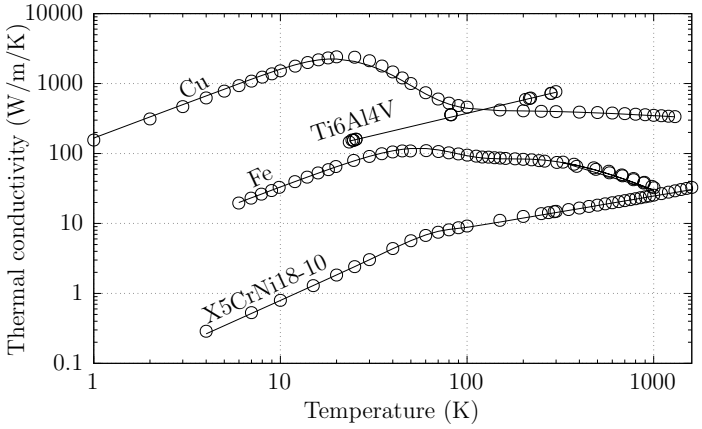


Figure 3: Temperature dependence of the thermal conductivity of several metallic materials. Dots correspond to the experimental data taken from (Touloukian and Ho, 1977; Godfrey *et al.*, 1964; Hust, 1969, 1984). Numerical data obtained from Equations (67) (copper and iron), (70) (X5CrNi18-10 stainless steel) and (71) (Ti6Al4V alloy) are represented with solid lines.

An alternative option consists of using the following expression to consider the temperature dependence of heat conductivity:

$$\kappa = \exp\left[-\left(\frac{T}{K_5}\right)^{K_6}\right] K_1 T^{K_2} + \left(1 - \exp\left[-\left(\frac{T}{K_5}\right)^{K_6}\right]\right) K_3 T^{K_4} \qquad (70)$$

The above expression assumes that the impact of temperature on thermal conductivity is the weighted sum of two power functions. While the former dominates the low temperature behavior ($T < K_5$), the latter controls the high temperature behavior ($T > K_5$).

Finally, in some cases, a single power function provides a reasonable description of the impact on temperature on thermal conductivity:

$$\kappa = K_1 T^{K_2} \qquad (71)$$

Such a function, which requires only two material parameters, is a specific case of (70) for which the $K_5$ takes an infinite value.

The thermal conductivities of different materials are plotted as a function of temperature in Figure 3. For pure metals (Fe and Cu), the impact of temperature is correctly depicted with Equation (67). It is worth mentioning that for pure metals, the thermal conductivity at low temperatures

depends on the concentration of defects. As a consequence, the $K_0$ parameter, which controls the low temperature behavior, should be adjusted for each specific situation. For metallic alloys, the temperature-dependence of thermal conductivity is reasonably described with either Equation (70) (e.g., X2CrNi18-9) or (71) (e.g., Ti6Al4V).

*2.7.4. Stiffness properties*

As discussed by Ledbetter (1982), the impact of temperature on the Young's modulus of most metallic materials can be represented by the relation proposed by Varshni (1970):

$$E = E_0 \left( 1 - \frac{E_1 T_e}{\exp[T_e/T] - 1} \right) \tag{72}$$

An alternative strategy to describe the temperature dependence of stiffness properties consists of using the expression proposed by Wachtman *et al.* (1961):

$$E = E_0 \left( 1 - E_1 T \exp\left[ -\frac{T_e}{T} \right] \right) \tag{73}$$

In the above equations, $E_0$, $E_1$ and $T_e$ are material parameters. Specifically, $E_0$ is the Young's modulus at absolute zero, $T_e$ is a characteristic temperature and $E_1$ controls the derivative of the Young's modulus with respect to temperature when temperature approaches infinity. The above relations, which can be applied to other elastic constants (e.g., bulk modulus, shear modulus), are consistent with the third law of thermodynamics in the sense that the derivative with respect to temperature vanishes at absolute zero. Also, they both rely on the assumption that the stiffness properties exhibit an affine relationship with respect to temperature in the high temperature regime. It is worth mentioning that Li *et al.* (2019) proposed a temperature-dependent elastic modulus model that uses a limited number of parameters. According to this model, both the specific heat capacity and the thermal expansion coefficient need to be integrated with respect to temperature for the evaluation of the Young's modulus. While such a method correctly reproduces the impact of temperature on stiffness properties for many metallic materials, the integration of thermophysical properties may require some numerical procedures that can be computationally expensive.

As illustrated by Figure 4, the approximation of Wachtman *et al.* (1961) (see Equation (73)) provide an accurate description of the temperature-

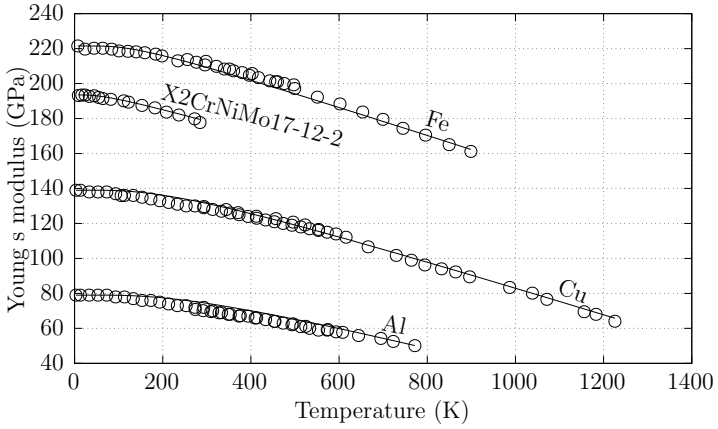


Figure 4: Temperature dependence of the linear thermal expansion coefficient of several metallic materials. Dots correspond to the experimental data taken from (Köster, 1948a,b; Ledbetter, 1982; Zhang *et al.*, 1991; Adams *et al.*, 2006; Isaak and Masuda, 1995). Numerical data obtained from Equation (73) is represented with solid lines.

dependence of the Young's modulus of pure metals and alloys. Very similar results are obtained with Equation (72), which differ from Equation (73) only in the intermediate temperature range. It should be mentioned that for ferromagnetic materials, some deviations with respect to Equations (72) and (73) can be observed as a result of magnetostrictive effects.

## 3. Application to polycrystalline copper

For the purpose of illustration, the present framework is used to construct a set of constitutive relations for polycrystalline copper. In this section, the constitutive relations are first detailed. The corresponding material parameters are then presented. The proposed constitutive model is finally used to discuss the thermodynamical implications of some deformation processes.

### *3.1. Constitutive equations*

For isotropic stiffness properties, the stiffness tensor $\mathbb{C}$ is conveniently expressed from the bulk modulus $K$ and the shear modulus $G$ with

$$\mathbb{C} = 3K\mathbb{P}_s + 2G\mathbb{P}_d \tag{74}$$

where $\mathbb{P}_s$ (respectively $\mathbb{P}_d$) is the spherical (respectively deviatoric) fourth-rank projection tensor. To consider the impact of temperature on stiffness

properties, the relation proposed by Wachtman *et al.* (1961) is adopted:

$$K = K_0 \left(1 - K_1 T \exp\left[-\frac{T_e}{T}\right]\right) \tag{75}$$

$$G = G_0 \left(1 - G_1 T \exp\left[-\frac{T_e}{T}\right]\right) \tag{76}$$

Also, in the context of isotropy, the stress-free thermal expansion tensor $\bar{\boldsymbol{\alpha}}$ is obtained from the linear thermal expansion coefficient $\bar{\alpha}$ with:

$$\bar{\boldsymbol{\alpha}} = \bar{\alpha}\mathbf{1} \tag{77}$$

For polycrystalline copper, the temperature dependence of the linear thermal expansion coefficient is correctly described by Equation (66) with a first order polynomial function i.e., $n_\alpha = 1$.

To construct the viscoplastic flow rule, the equivalent stress is evaluated according to the definition of von Mises. In the absence of kinematic hardening, the von Mises equivalent stress is given by:

$$\Sigma_{eq} = \sqrt{\frac{3}{2}\boldsymbol{\Sigma}_d : \boldsymbol{\Sigma}_d} \tag{78}$$

where $\boldsymbol{\Sigma}_d$ is the deviatoric stress tensor. The differentiation of the equivalent stress with respect to the stress tensor leads to the following expression of the flow direction $\boldsymbol{N}$:

$$\boldsymbol{N} = \frac{3}{2}\frac{\boldsymbol{\Sigma}_d}{\Sigma_{eq}} \tag{79}$$

To consider the temperature-dependence of strain hardening, the hardening modulus $H$ is assumed to follow a similar trend as for the elastic constants:

$$H = H_0 \left(1 - H_1 T \exp\left[-\frac{T_h}{T}\right]\right) \tag{80}$$

where $H_0$, $H_1$ and $T_h$ are material parameters.

To evaluate the plastic multiplier, the flow rule of Chaboche (1989) is adopted:

$$\dot{P} = \dot{P}_0 \left(\frac{\langle \Sigma_{eq} - R \rangle}{B}\right)^{1/m} \tag{81}$$

where $\dot{P}_0$ is a reference plastic strain rate, $m$ is the strain-rate sensitivity exponent and $B$ is a reference stress. The effect of temperature on strain-rate sensitivity is depicted by the following relation:

$$m = M_0 + M_1 \left( \frac{T}{T_m} \right)^{M_2} \tag{82}$$

According to the above equation, the strain-rate sensitivity exponent at absolute zero is given by $M_0$ while the $M_1$ and $M_2$ material parameters control the temperature-dependency of the strain-rate sensitivity exponent. Also, $T_m$ is the melting temperature. To consider the dependence of the reference stress with respect to temperature, a similar expression as for the hardening modulus is adopted:

$$B = B_0 \left( 1 - H_1 T \exp \left[ -\frac{T_h}{T} \right] \right) \tag{83}$$

where $B_0$ is the reference stress at absolute zero.

The von Mises equivalent stress thus takes the following form:

$$\Sigma_{eq} = HZ + B \left( \frac{\dot{P}}{\dot{P}_0} \right)^m \quad \text{if } \dot{P} > 0 \tag{84}$$

$$= \left( H_0 Z + B_0 \left( \frac{\dot{P}}{\dot{P}_0} \right)^m \right) \left( 1 - H_1 T \exp \left[ -\frac{T_h}{T} \right] \right) \quad \text{if } \dot{P} > 0 \tag{85}$$

As indicated by the above Equation, the flow rule provided by Equation (81) is additive in the sense that the equivalent stress is given by the sum of strain and strain rate hardening contributions. However, the effect of temperature is included in a single factor that affects both contributions.

The evolution equation for the isotropic hardening variable includes both strain hardening and static recovery effects:

$$\dot{Z} = \begin{cases} \dot{P} - S \langle \frac{T - T_r}{T_m} \rangle^q Z^l, & Z < Z_c \\ \dot{P} \left( \frac{Z}{Z_c} \right)^{\frac{n-1}{n}} - S \langle \frac{T - T_r}{T_m} \rangle^q Z^l, & Z \geq Z_c. \end{cases} \tag{86}$$

where $Z_c$, $S$, $T_r$, $n$, $q$ and $l$ are positive material parameters. Specifically, $Z_c$ controls the transition from a linear hardening rule to a power hardening rule and $n$ is the strain hardening exponent. It is worth mentioning that such a

hardening rule is compatible with the second law of thermodynamics in the sense that the intrinsic contribution to the dissipation source is necessarily non-negative provided that the strain hardening exponent $n$ is inferior to unity. Also, $T_r$ is the minimum temperature for static recovery to occur.

The numerical procedure used for the time integration of constitutive relations relies on the second order Runge-Kutta method. It is briefly detailed in Appendix A.

*3.1.1. Parameter identification*

The material parameters for polycrystalline copper are listed in Table 2. The bulk and shear moduli were taken from the experimental data of Ledbetter (1981). The experimental data of Johnson (1960), Touloukian *et al.* (1975) and White and Collocott (1984) were used to obtain the linear thermal expansion coefficient and specific heat capacity at zero stress. Also, the viscoplastic and strain hardening parameters were adjusted to fit the experimental data of Chen and Kocks (1991) who conducted uniaxial tension tests at different temperatures (from 293 K to 673 K) and different strain rates ($10^{-4}$ and 1 $s^{-1}$). The corresponding results are plotted in Figure 5. Finally, the static recovery parameters were determined from the results of McQueen and Vazquez (1986). Specifically, uniaxial compression tests were conducted at 723 K up to an axial strain of -15% with a constant strain rate of -0.18 $s^{-1}$, interrupted and resumed. The experimental results were then used to evaluate the softening ratio $X_s$ such that:

$$X_s = \frac{\Sigma_m - \Sigma_r}{\Sigma_m - \Sigma_0} \tag{87}$$

where $\Sigma_m$ is the maximum equivalent stress obtained for an axial strain of -15%, $\Sigma_0$ is the initial yield stress and $\Sigma_r$ is the yield stress obtained upon reloading. The softening ratios obtained for different interruption times are plotted in Figure 6.

*3.1.2. Discussion*

*Heat sources.* To evaluate the contributions of the different heat sources to the heat diffusion equation, the behavior of polycrystalline copper under simple shear was evaluated. Specifically, a constant logarithmic shear strain rate of 1 $s^{-1}$ was imposed and isothermal conditions, with a temperature of either 73 K or 673 K, were considered.

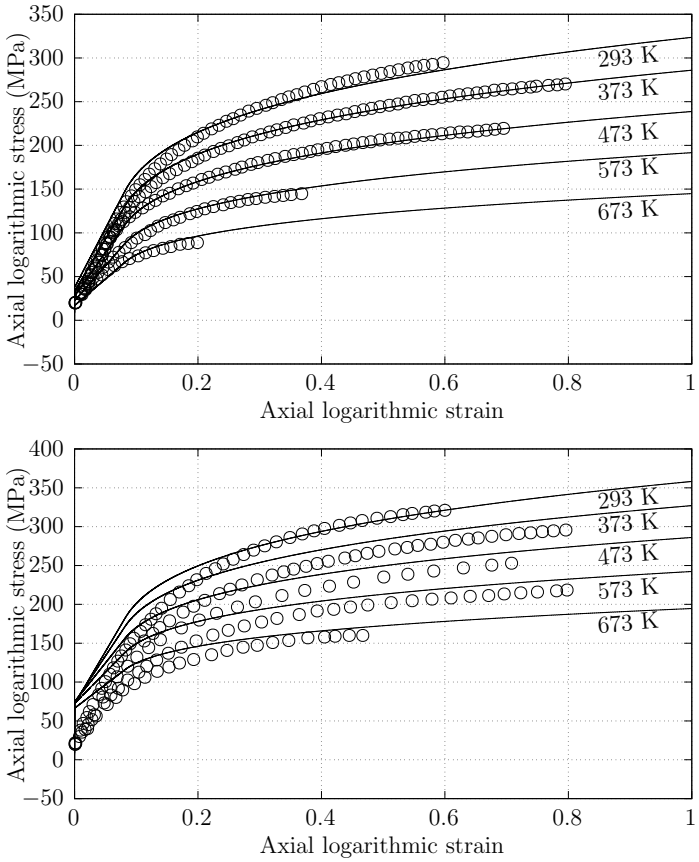


Figure 5: Logarithmic stress-strain curves obtained for polycrystalline copper under uniaxial tension at different temperatures with a strain rate of either $10^{-4}$ $s^{-1}$ (top) or 1 $s^{-1}$ (bottom). Dots correspond to the experimental data of Chen and Kocks (1991). Numerical data obtained from the present model is represented with solid lines.

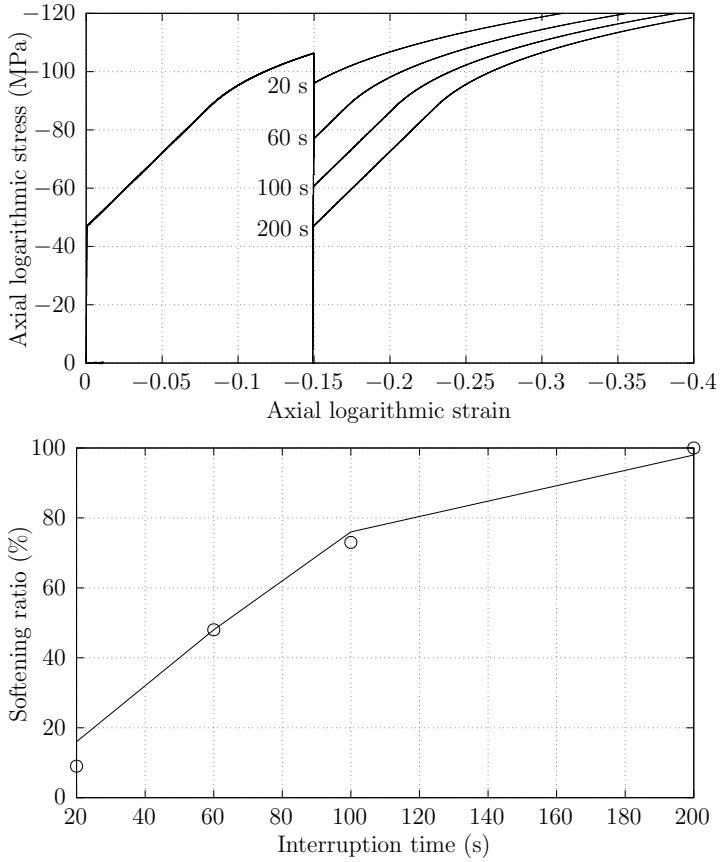


Figure 6: Logarithmic stress-strain curves obtained for polycrystalline copper under uniaxial compression at 723 K with a strain rate of 0.18 $s^{-1}$ and different interruption times (top). Evolution of the softening ratio as a function of the interruption time (bottom). Dots correspond to the experimental data of McQueen and Vazquez (1986). Numerical data obtained from the present model is represented with solid lines.

| | | | |
|---|---|---|---|
| $K_0$ (GPa) | $K_1$ ($K^{-1}$) | $G_0$ (GPa) | $G_1$ ($K^{-1}$) |
| 145 | $5.68 \times 10^{-4}$ | 52 | $5.68 \times 10^{-4}$ |
| $T_e$ (K) | $T_d$ (K) | $T_m$ (K) | $T_h$ (K) |
| 343 | 343 | 1358 | 100 |
| $T_r$ (K) | $M_0$ | $M_1$ | $M_2$ |
| 673 | 0.01 | 0.28 | 1 |
| $A_\infty$ ($K^{-1}$) | $A_1$ ($K^{-2}$) | $C_\infty$ (J/kg/K) | $C_1$ (J/kg/$K^2$) |
| $1.8 \times 10^{-5}$ | $2 \times 10^{-9}$ | 390 | $5 \times 10^{-6}$ |
| $H_0$ (MPa) | $H_1$ ($K^{-1}$) | $n$ | $Z_c$ |
| 1800 | $1.12 \times 10^{-3}$ | 0.25 | 0.08 |
| $S$ | $q$ | $l$ | $\varrho_0$ (kg/$m^3$) |
| $3.12 \times 10^{-2}$ | 1 | 0.25 | 8960 |
| $B_0$ (MPa) | $\dot{P}_0$ ($s^{-1}$) | | |
| 50 | $1 \times 10^{-4}$ | | |

Table 2: Material parameters for polycrystalline copper.

The evolutions of the intrinsic dissipation source, thermoelastic heat source and internal coupling heat source are presented in Figure 7 for both temperatures. According to the results, at low temperature (73 K), the thermoelastic and internal coupling heat sources are negligible in comparison with the intrinsic dissipation source. For many practical situations, the temperature evolution can thus be correctly approximated by solely considering the intrinsic dissipation source. However, at high temperature, as a result of the temperature-dependence of hardening properties, the internal coupling heat source becomes significant, especially at moderate strains where the hardening variable rate is important.

The differential Taylor-Quinney coefficient $\beta$ is plotted as a function of the shear strain in Figure 8. Two distinct stages are observed. In the first stage, where the hardening rule is linear (i.e., $Z \leq Z_c$), the differential Taylor-Quinney coefficient decreases and reaches a minimal value. This effect is due to the fact that a significant part of the plastic work rate is stored as internal energy because of the important hardening rate. At high temperature (673 K), this effect is less pronounced due to the higher strain rate sensitivity. In the second stage (i.e., $Z > Z_c$), the hardening rule becomes non-linear and the hardening rate decreases with an increasing strain. An important augmentation of the differential Taylor-Quinney coefficient is therefore observed.

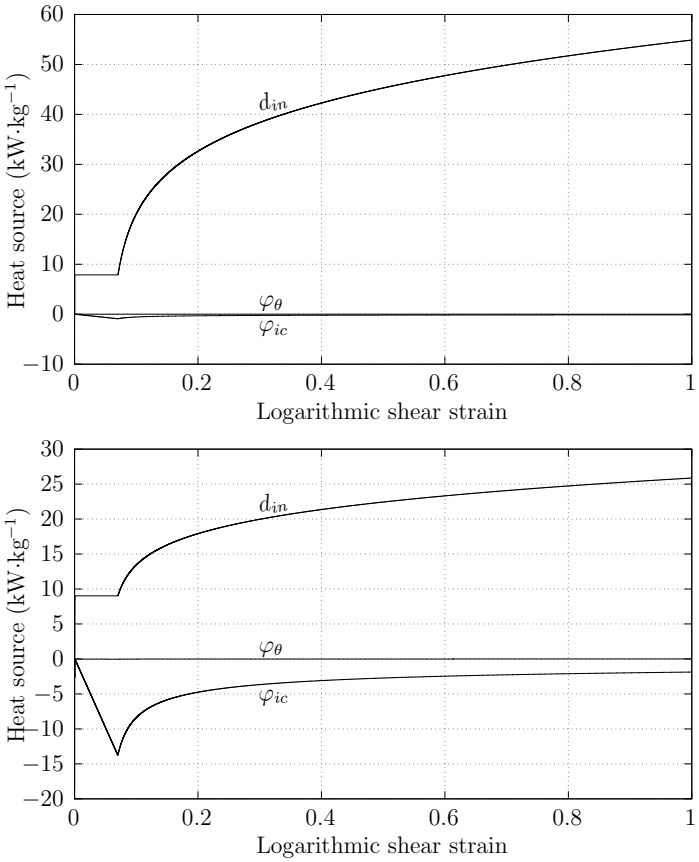


Figure 7: Evolution of the intrinsic dissipation source, thermoelastic heat source and internal coupling heat source for polycrystalline copper under simple shear with a shear strain rate of 1 $s^{-1}$ and a temperature of either 73 K (top) or 673 K (bottom).

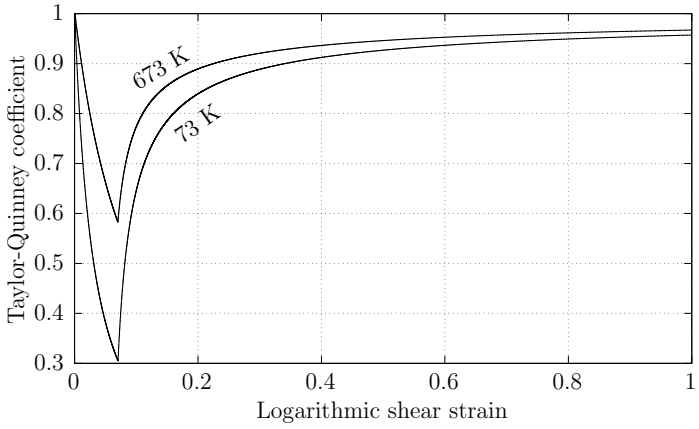


Figure 8: Evolution of the differential Taylor-Quinney coefficient for polycrystalline copper under simple shear with a shear strain rate of 1 $s^{-1}$ and a temperature of either 73 K or 673 K.

For important plastic strains, the Taylor-Quinney coefficient is close to unity, which indicates that most of the plastic work is dissipated into heat.

*Thermophysical properties.* To determine how the specific heat capacity and the thermal expansion coefficient are impacted by a deformation process, the behavior of polycrystalline copper under uniaxial compression was examined. As for the simple shear test, isothermal conditions were prescribed with a constant temperature of either 73 or 673 K and the axial strain rate was fixed to $-1$ $s^{-1}$.

The evolution of the specific heat capacities at constant strain or constant stress as a function of the axial strain are presented in Figure 9. Whatever the temperature is, the specific heat capacities at constant strain $c_v$ and $\bar{c}_v$ are close to each other. As a result, for many practical applications, the specific heat capacity at constant strain $c_v$, which appears in the heat diffusion equation, can advantageously be replaced by that obtained in the absence of external stress and hardening $\bar{c}_v$. Indeed, as indicated by Equation (31), while the former depends on the internal state, the latter only depends on the absolute temperature.

The linear thermal expansion coefficients along and perpendicular to the loading direction direction, respectively denoted by $\alpha_{\parallel}$ and $\alpha_{\perp}$, are reported in Figure 10. The stress-free linear thermal expansion coefficient $\bar{\alpha}$ is also displayed. At low temperature (73 K), since stiffness properties do not signif-

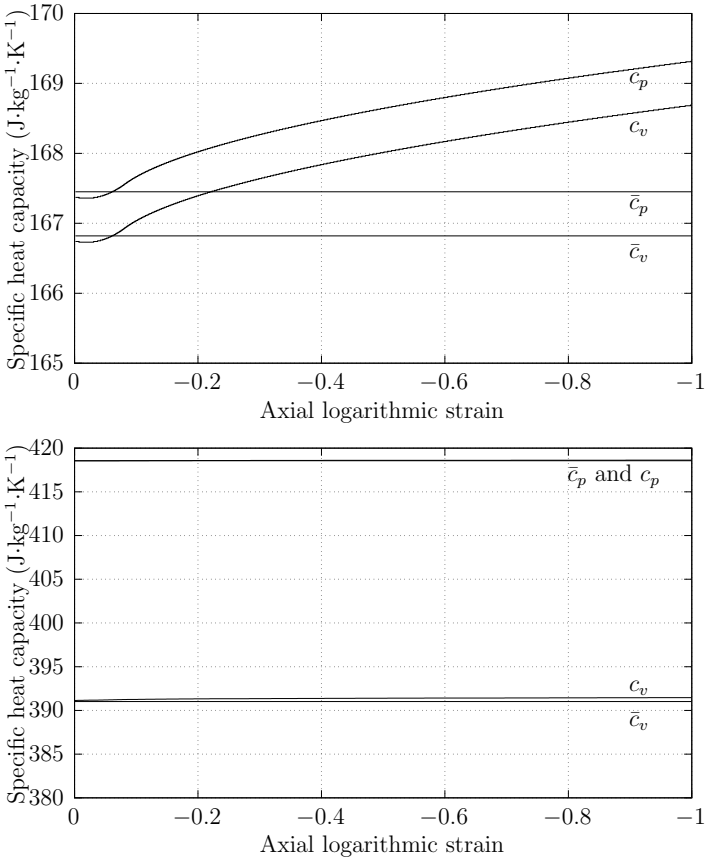


Figure 9: Evolution of the specific heat capacity for polycrystalline copper under uniaxial compression with an axial strain rate of $-1$ s$^{-1}$ and a temperature of either 73 K (top) or 673 K (bottom).

icantly depend on temperature, no major difference is observed between the different linear thermal expansion coefficients. However, at high temperature (673 K), the discrepancies between the stress-free and current linear thermal expansion coefficients cannot be neglected.

## 4. Conclusions

A general framework dedicated to the development of constitutive models for metallic materials was proposed in the present paper. The proposed framework is dedicated to applications involving important temperature variations. The main features of the framework are:

- The additive decomposition of the logarithmic strain tensor is adopted to include the contributions of elasticity, plasticity and thermal expansion to deformation.
- The classical internal variable concept is used to consider the history effects associated with the development of plasticity, which includes strain hardening, static recovery and dynamic recovery.
- The temperature dependence of common thermophysical properties is considered. Some equations, which are in agreement with the third law of thermodynamics, have been proposed to reproduce the effect of temperature on these properties.

For the purpose of illustration, the proposed framework was used to build a constitutive model for polycrystalline copper. Such a model allows discussing the impact of thermomechanical couplings on the deformation behavior over a wide temperature range. The results indicate that:

- While the thermoelastic heat source remains negligible in comparison with the intrinsic dissipation, the role of the internal coupling heat source, which results from the temperature-dependence of hardening properties, cannot be ignored at high temperature.
- The contribution of hardening to the specific heat capacity at constant strain is negligible. This contribution can therefore be ignored for many practical applications for which the solution to heat diffusion equation is needed.

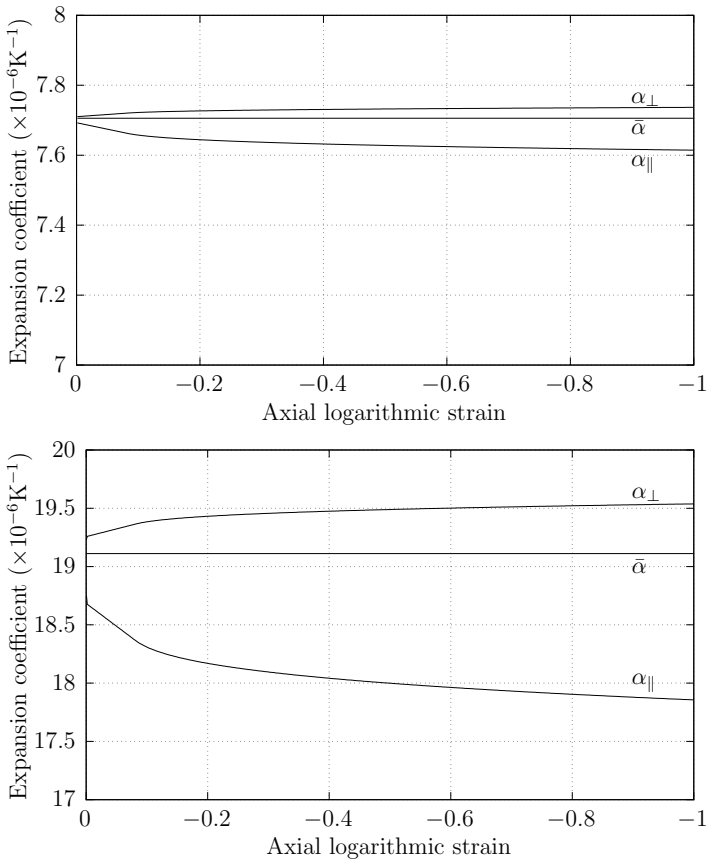


Figure 10: Evolution of the linear thermal expansion for polycrystalline copper under uniaxial compression with an axial strain rate of $-1$ s$^{-1}$ and a temperature of either 73 K (top) or 673 K (bottom). The linear thermal expansion coefficient parallel and perpendicular to the loading direction are respectively denoted by $\alpha_\parallel$ and $\alpha_\perp$. The stress-free linear thermal expansion coefficient is denoted by $\bar{\alpha}$.

It is important to mention that the proposed framework does not include any length scale. As a consequence, the resulting constitutive models cannot provide satisfying predictions for strain localization, which may occur when softening is present. To limit localization, a possible strategy would consist of treating the spatial gradients (Mühlhaus and Aifantis, 1991; Geers, 2004; Miehe, 2014) or the spatial average and/or variance (Mareau, 2022) of plastic strain measures as additional state variables. Also, future work should focus on the description of the effect of temperature on damage, which is an important aspect of the processing of metallic materials.

## Appendix A. Numerical implementation

The numerical implementation of constitutive equations is detailed hereafter. The objective of this implementation is twofold. First, for a prescribed loading path, it aims at integrating the evolution equations. For this purpose, each loading path is decomposed into time increments. The integration procedure then uses the temperatures and deformation gradient tensors at the beginning ($t$) and the end of the time increment ($t + \Delta t$), as well as the internal variables at the beginning of the time increment, to determine the internal variables and the applied stress tensor at the end of the time increment. In the present work, a second order Runge-Kutta integration method is used to integrate the evolution equations. For the application of this method, both the logarithmic strain tensor and the absolute temperature in the middle of the time increment should be known. They are computed according to:

$$\boldsymbol{E}[t + \Delta t/2] = \frac{1}{2}\left(\boldsymbol{E}[t + \Delta t] + \boldsymbol{E}[t + \Delta t]\right) \tag{A.1}$$

$$T[t + \Delta t/2] = \frac{1}{2}\left(T[t + \Delta t] + T[t + \Delta t]\right) \tag{A.2}$$

Second, the numerical procedure allows controlling the prescribed deformation gradient tensor. Specifically, the integration of constitutive relations assumes that the deformation gradient tensor at the end of a time increment is known. However, for stress-controlled or mixed loading conditions, the deformation gradient tensor at the end of the time increment is not available. To circumvent this difficulty, an iterative procedure is used. It consists of adjusting the deformation gradient tensor to obtain, within a given tolerance,

the prescribed stress state. At the beginning of each iteration, the prescribed deformation gradient tensor is estimated with:

$$\boldsymbol{F}_{ij}[t+\Delta t] = \boldsymbol{F}^{bc}_{ij}[t+\Delta t]\left(1-\boldsymbol{\eta}_{ij}\right) + \frac{\boldsymbol{P}^{bc}_{ij}[t+\Delta t] - \boldsymbol{P}_{ij}[t+\Delta t]}{D}\boldsymbol{\eta}_{ij} \quad \text{(A.3)}$$

where $\boldsymbol{F}^{bc}$ is the prescribed deformation gradient tensor, $\boldsymbol{P}^{bc}$ is the prescribed first Piola-Kirchoff stress tensor and $D$ is a numerical parameter that controls the convergence rate. Also, $\boldsymbol{\eta}$ is a matrix that indicates whether a given component $\boldsymbol{P}_{ij}$ of the Piola-Kirchoff stress tensor is prescribed ($\boldsymbol{\eta}_{ij} = 1$) or not ($\boldsymbol{\eta}_{ij} = 0$). To determine whether convergence is achieved or not, the difference $\epsilon$ between the actual and prescribed stress tensor is calculated according to:

$$\epsilon = \sqrt{\sum_{i,j} \boldsymbol{\eta}_{ij}\left(\boldsymbol{P}^{bc}_{ij} - \boldsymbol{P}_{ij}\right)^2} \quad \text{(A.4)}$$

Convergence is achieved when the difference $\epsilon$ is inferior to a given tolerance $\epsilon_{bc}$. The numerical implementation of the constitutive model is briefly described in Table A.3.

## References


Adams, J.J., Agosta, D.S., Leisure, R.G., Ledbetter,H., 2006. Elastic constants of monocrystal iron from 3 to 500K. Journal of Applied Physics 100(11). https://doi.org/10.1063/1.2365714

Benallal, A., Bigoni, D., 2004. Effects of temperature and thermo-mechanical couplings on material instabilities and strain localization of inelastic materials. Journal of the Mechanics and Physics of Solids 52(3). https://doi.org/10.1016/S0022-5096(03)00118-2

Brooks, C.R., Bingham, R.E., 1968. The specific heat of aluminum from 330 to 890°K and contributions from the formation of vacancies and anharmonic effects. Journal of Physics and Chemistry of Solids 29(9), 1553–1560. https://doi.org/10.1016/0022-3697(68)90097-8

Caminero, M.A., Montáns, F.J., Bathe, K-J., 2011. Modeling large strain anisotropic elasto-plasticity with logarithmic strain and stress measures, Computers & Structures 89(11–12), 826–843. https://doi.org/10.1016/j.compstruc.2011.02.011

▷ Set the state variables to their initial values
**For** each time $t$:
  **Do while** $\epsilon > \epsilon_{bc}$:
    ▷ Compute the deformation gradient tensor at time $t + \Delta t$
    $\rightarrow \boldsymbol{F}[t + \Delta t]$
    ▷ Compute the logarithmic strain tensor at time $t$
    $\rightarrow \boldsymbol{E}[t]$
    ▷ Compute the logarithmic strain tensor at time $t + \Delta t$
    $\rightarrow \boldsymbol{E}[t + \Delta t]$
    ▷ Compute the logarithmic strain tensor at time $t + \Delta t/2$
    $\rightarrow \boldsymbol{E}[t + \Delta t/2]$
    ▷ Compute the absolute temperature at time $t + \Delta t/2$
    $\rightarrow T[t + \Delta t/2]$
    ▷ Compute the stress tensors at time $t$
    $\rightarrow \boldsymbol{\Sigma}[t]$ and $\boldsymbol{\chi}[t]$
    ▷ Compute the yield stress increase at time $t$
    $\rightarrow R[t]$
    ▷ Integrate evolution equations between $t$ and $t + \Delta t/2$
    $\rightarrow \boldsymbol{E}_p[t + \Delta t/2]$, $\boldsymbol{A}[t + \Delta t/2]$ and $Z[t + \Delta t/2]$
    ▷ Compute the stress tensors at time $t + \Delta t/2$
    $\rightarrow \boldsymbol{\Sigma}[t + \Delta t/2]$ and $\boldsymbol{\chi}[t + \Delta t/2]$
    ▷ Compute the yield stress increase at time $t + \Delta t/2$
    $\rightarrow R[t + \Delta t/2]$
    ▷ Integrate evolution equations between $t + \Delta t/2$ and $t + \Delta t$
    $\rightarrow \boldsymbol{E}_p[t + \Delta t]$, $\boldsymbol{A}[t + \Delta t]$ and $Z[t + \Delta t]$
    ▷ Compute the stress tensors at time $t + \Delta t$
    $\rightarrow \boldsymbol{\Sigma}[t + \Delta t]$ and $\boldsymbol{\chi}[t + \Delta t]$
    ▷ Compute the yield stress increase at time $t + \Delta t$
    $\rightarrow R[t + \Delta t]$
    ▷ Compute the specific internal energy at time $t + \Delta t$
    $\rightarrow e[t + \Delta t]$
    ▷ Compute the heat sources at time $t + \Delta t$
    $\rightarrow d_{in}[t + \Delta t]$, $\varphi_\theta[t + \Delta t]$ and $\varphi_{ic}[t + \Delta t]$
    ▷ Compute the first Piola-Kirchoff stress tensor at time $t + \Delta t$
    $\rightarrow \boldsymbol{P}[t + \Delta t]$
    ▷ Compute the difference
    $\rightarrow \epsilon$

Table A.3: Numerical integration of constitutive relations for a prescribed loading path.

Cezairliyan, A., Touloukian, Y.S., 1965. Correlation and prediction of thermal conductivity of metals through the application of the principle of corresponding states, in: Advances in Thermophysical Properties at Extreme Temperatures and Pressures, Third Symposium on Thermoohysical Properties, ASME, 301–313.

Chaboche, J.L., 1989. Constitutive equations for cyclic plasticity and cyclic viscoplasticity. International Journal of Plasticity 5(3), 247–302. https://doi.org/10.1016/0749-6419(89)90015-6

Chen, S.R., Kocks, U.F., 1991. High-temperature plasticity in copper polycrystals, in: Freed A.D., Walker, K.P. (Eds), High temperature constitutive modelling. New York: Am. Soc. Mech. Eng. 1.

Debye, P., 1912. Zur Theorie der spezifischen Wärmen. Ann. Phys. 344(14). https://doi.org/10.1002/andp.19123441404

Egner, H., Egner, W., 2014. Modeling of a tempered martensitic hot work tool steel behavior in the presence of thermo-viscoplastic coupling. International Journal of Plasticity 57. https://doi.org/10.1016/j.ijplas.2014.03.002

Geers, M.G.D., 2004. Finite strain logarithmic hyperelasto-plasticity with softening: a strongly non-local imlicit gradient framework. Computer Methods in Applied Mechanics and Engineering 193, 3377–3401. https://doi.org/10.1016/j.cma.2003.07.014

Godfrey, T.G., Fulkerson, W., Kollie, T.G., Moore, J.P., McElroy, D.L., 1964. Thermal Conductivity of Uranium Dioxide and Armco Iron by an Improved Radial Heat Flow Technique, U.S.A.E.C. Rep. 0RNL-3556, 1–67.

Harzallah, M., Pottier, T., Gilblas, R., Landon, Y., Mousseigne, M., Senatore, J., 2018. A coupled in-situ measurement of temperature and kinematic fields in Ti-6Al-4V serrated chip formation at micro-scale. International Journal of Machine Tools and Manufacture 130–131, 20–35. https://doi.org/10.1016/j.ijmachtools.2018.03.003

Hencky, H., 1928. Über die Form des Elastizit ätsgesetzes bei ideal elastischen Stoffen. Zeitschrift für technische Physik 9, 215–220.

Houlsby, G.T., Puzrin, A.M., 2000. A thermomechanical framework for constitutive models for rate-independent dissipative materials. International Journal of Plasticity 16(9), 1017–1047. https://doi.org/10.1016/S0749-6419(99)00073-X

Hust, J.G., 1969. Thermal Conductivity Standard Reference Materials from 4 to 300 K. I. Armco Iron, National Bureau of Standards, Boulder, Colo., Report No. 9740.

Hust, J.G., 1984. Thermal Conductivity of Aluminum, Copper, Iron, and Tungsten for Temperatures from 1 K to the Melting Point. National Institute of Standards and Technology (NIST). https://www.govinfo.gov/app/details/GOVPUB-C13-5dca61206b094d8b3a54099ebcff1baa

Isaak, D.G., Masuda, K., 1995. Elastic and viscoelastic properties of $\alpha$ iron at high temperatures. Journal of Geophysical Research: Solid Earth 100(B9). https://doi.org/10.1029/95JB01235

Johnson, V.J., 1960. A compendium of the properties of materials at low temperature (Phase I). Part II. Properties of solids.

Kim, C.S, 1975. Thermophysical properties of stainless steels. https://www.osti.gov/biblio/4152287.

Köster, W., 1948. The temperature dependence of the elasticity modulus of pure metals. Z . Metallkd. 39, 1–9.

Köster, W., 1948. Uber eine Sondererscheinung im Temperaturgang von Elastizitatsmodul und Dämpfung der Metalle Kupfer, Silber, Aluminium und Magnesium. Z. Metallkd. 39, 9–12.

Ledbetter, H.M., 1981. Elastic Constants of Polycrystalline Copper at Low Temperatures. Phys. Stat. Sol. (a) 66, 477–484. https://doi.org/10.1002/pssa.2210660209

Ledbetter, H.M., 1982. Temperature behaviour of Young's moduli of forty engineering alloys, Cryogenics 22(12), 653–656. https://doi.org/10.1016/0011-2275(82)90072-8

Li, W., Kou, H., Zhang, X., Ma, J., Li, Y., Geng, P., Wu, X., Chen, L., Fang, D., 2019. Temperature-dependent elastic modulus model for metallic bulk

materials. Mechanics of Materials 139, 1–7. https://doi.org/10.1016/j.mechmat.2019.103194

Mareau, C., 2020. A thermodynamically consistent formulation of the Johnson–Cook model. Mechanics of Materials 143. https://doi.org/10.1016/j.mechmat.2020.103340

Mareau, C., 2022. Thermodynamic framework for variance-based non-local constitutive models. Continuum Mechanics and Thermodynamics 34, 1173–1195. https://doi.org/10.1007/s00161-022-01113-8

Maugin, G.A., Muschik, W., 1994. Thermodynamics with Internal Variables. Part I. General Concepts. J. Non-Equilib. Thermodyn. 19, 217–249.

McQueen H.J., Vazquez, L., 1986. Static Recovery of Copper during Annealing and Stress Relaxation following Hot Deformation. Materials Science and Engineering 81, 355–369. https://doi.org/10.1016/0025-5416(86)90275-2

Miehe, C., Apel, N., Lambrecht, M., 2002. Anisotropic additive plasticity in the logarithmic strain space: modular kinematic formulation and implementation based on incremental minimization principles for standard materials. Computer Methods in Applied Mechanics and Engineering 191(47–48), 5383–5425. https://doi.org/10.1016/S0045-7825(02)00438-3

Miehe, C., 2014. Variational gradient plasticity at finite strains. Part I: Mixed potentials for the evolution and update problems of gradient-extended dissipative solids. Computer Methods in Applied Mechanics and Engineering 268, 677–703. https://doi-org/10.1016/j.cma.2013.03.014

Miločević, N., Aleksić, I., 2012. Thermophysical properties of solid phase Ti-6Al-4V alloy over a wide temperature range. Int. J. Mat. Res. 103, 707–714. https://doi.org/10.3139/146.110678

Mühlhaus, H.-B., Aifantis, E.C., 1991. A variational principle for gradient plasticity. Int. J. Solids Struct. 28, 845–857. https://doi.org/10.1016/0020-7683(91)90004-Y

Nguyen, Q.S., 2000. Stability and Nonlinear Solid Mechanics, John Wiley & Sons Ltd, Chichester.

Papadopoulos, P., Lu, J., 2001. On the formulation and numerical solution of problems in anisotropic finite plasticity. Computer Methods in Applied Mechanics and Engineering 190, 4889–4910. https://doi.org/10.1016/S0045-7825(00)00355-8

Papenfuß, C., 2020. Continuum Thermodynamics and Constitutive Theory. Springer, Cham.

Rittel, D., Zhang, L.H., Osovski, S., 2017. The dependence of the Taylor–Quinney coefficient on the dynamic loading mode. Journal of the Mechanics and Physics of Solids 107, 96–114. https://doi.org/10.1016/j.jmps.2017.06.016

Sansour, C., Wagner, W., 2003. Viscoplasticity based on additive decomposition of logarithmic strain and unified constitutive equations: Theoretical and computational considerations with reference to shell applications. Computers & Structures 81, 1583–1594. https://doi.org/10.1016/S0045-7949(03)00149-4

Shaw, M.C., 2005. Metal Cutting Principles. Oxford University Press, New York, Oxford.

Simo, J.C., Miehe, C., 1992. Associative coupled thermoplasticity at finite strains: Formulation, numerical analysis and implementation. Computer Methods in Applied Mechanics and Engineering 98(1), 41–104. https://doi.org/10.1016/0045-7825(92)90170-O

Tang, M., Pan, X., Zhang, M., Wen, H., 2021. Scaling Behavior between Heat Capacity and Thermal Expansion in Solids. Chin. Phys. Lett. 38. https://dx.doi.org/10.1088/0256-307X/38/2/026501

Taylor, G.I., Quinney, H., 1934. The latent energy remaining in a metal after cold working. Proc. R. Soc. London 143, 307–326.

Touloukian, Y.S., Kirby, R.K., Taylor, R.E., Desai, P.D., 1975. Thermophysical properties of matter - the TPRC data series. Volume 12. Thermal expansion metallic elements and alloys. (Reannouncement). Data book. United States: N. p., 1975. Web.

Touloukian, Y.S., Ho, C.Y., 1977. Thermophysical Properties of Selected Aerospace Materials. Part 2. Thermophysical Properties of Seven Materials, Defense technical information center.

Varshni, Y.P., 1970. Temperature Dependence of the Elastic Constants. Phys. Rev. B 2(10). https://doi.org/10.1103/PhysRevB.2.3952

Valanis, K.C., 1971. Introduction. In: Irreversible Thermodynamics of Continuous Media. International Centre for Mechanical Sciences, vol 77. Springer, Vienna.

Wachtman Jr., J.B., Tefft, W.E., Lam, D.G., Apstein, C.S., 1961. Exponential temperature dependence of Young's modulus for several oxides, Physical Review 122, 1754–1759. https://doi.org/10.1103/PhysRev.122.1754

Wasserbäh, W., 1978. Low-temperature thermal conductivity of plastically deformed niobium single crystals. Philosophical Magazine A, 38(4), 401–431. https://doi.org/10.1080/01418617808239244

White, G.K., Collocott, S.J., 1984. Heat Capacity of Reference Materials: Cu and W. Journal of Physical and Chemical Reference Data 13(4), 1251–1257. https://doi.org/10.1063/1.555728

Xiao, H., Bruhns, O.T., Meyers, A., 2007. Thermodynamic laws and consistent Eulerian formulation of finite elastoplasticity with thermal effects. Journal of the Mechanics and Physics of Solids 55(2), 338–365. https://doi.org/10.1016/j.jmps.2006.07.005

Ziegler, W.T., Mullins, J.C., Hwa, S.C.P., 1963. Specific Heat and Thermal Conductivity of Four Commercial Titanium Alloys from 20° to 300°K, in: Timmerhaus, K.D. (Eds), Advances in Cryogenic Engineering, Springer US, Boston, MA, pp 268–277.

Zeng, C., Wen, H., Bernard, B.C., Raush, J.R., Gradl, P.R., Khonsari, M., Guo, S.M., 2021. Effect of temperature history on thermal properties of additively manufactured C-18150 alloy samples. Manufacturing Letters 28, 25–29. https://doi.org/10.1016/j.mfglet.2021.02.002

Zhang, J., Nyilas, A., Obst, B., 1991. New technique for measuring the dynamic Young's modulus between 295 and 6 K. Cryogenics 31(10), 884–889. https://doi.org/10.1016/0011-2275(91)90022-O

Zhang, M., Baxevanis, T., 2022. Tailoring the anisotropic (positive/zero/negative) thermal expansion in shape memory alloys through phase transformation and martensite (re)orientation. International Journal of Engineering Science 177, 1–15. https://doi.org/10.1016/j.ijengsci.2022.103687